

Geochemistry, Geophysics, Geosystems

RESEARCH ARTICLE

10.1002/2017GC007331

Special Section:

Magnetism in the Geosciences
- Advances and Perspectives

Key Points:

- The effect of 973 K heat treatment on magnetic and structural properties of experimentally shocked magnetite was studied
- Magnetic domain state is controlled by annealing of lattice defects during magnetite recrystallization
- These data contribute to the understanding of formation mechanisms of magnetic anomalies in large impact craters

Supporting Information:

- Supporting Information S1
- Table S1
- Data Set S1
- Data Set S2
- Data Set S3

Correspondence to:

A. Kontny,
agnes.kontny@kit.edu

Citation:

Kontny, A., Reznik, B., Boubnov, A., Göttlicher, J., & Steininger, R. (2018). Postshock thermally induced transformations in experimentally shocked magnetite. *Geochemistry, Geophysics, Geosystems*, 19, 921–931. <https://doi.org/10.1002/2017GC007331>

Received 8 NOV 2017

Accepted 27 FEB 2018

Accepted article online 12 MAR 2018

Published online 24 MAR 2018

Postshock Thermally Induced Transformations in Experimentally Shocked Magnetite

A. Kontny¹ , B. Reznik¹ , A. Boubnov², J. Göttlicher³, and R. Steininger³

¹Institute of Applied Geosciences, Karlsruhe Institute of Technology, Karlsruhe, Germany, ²SLAC National Accelerator Laboratory, Stanford Synchrotron Radiation Lightsource (SSRL), Menlo Park, CA, USA, ³Synchrotron Radiation Facility ANKA, Karlsruhe Institute of Technology, Eggenstein-Leopoldshafen, Germany

Abstract We studied the effect of 973 K heating in argon atmosphere on the magnetic and structural properties of a magnetite-bearing ore, which was previously exposed to laboratory shock waves between 5 and 30 GPa. For this purpose magnetic properties were studied using temperature-dependent magnetic susceptibility, magnetic hysteresis and low-temperature saturation isothermal remanent magnetization. Structural properties of magnetite were analyzed using X-ray diffraction, high-resolution scanning electron microscopy and synchrotron-assisted X-ray absorption spectroscopy. The shock-induced changes include magnetic domain size reduction due to brittle and ductile deformation features and an increase in Verwey transition temperature due to lattice distortion. After heating, the crystal lattice is relaxed and apparent crystallite size is increased suggesting a recovery of lattice defects documented by a mosaic recrystallization texture. The structural changes correlate with modifications in magnetic domain state recorded by temperature-dependent magnetic susceptibility, hysteresis properties and low-temperature saturation isothermal remanent magnetization. These alterations in both, magnetic and structural properties of magnetite can be used to assess impact-related magnetic anomalies in impact structures with a high temperature overprint.

1. Introduction

Hypervelocity impact events are widespread phenomena throughout the solar system and the interest in understanding shock demagnetization of crustal material has increased significantly in the last decade (e.g., Bezaeva et al., 2016; Gattacceca et al., 2007; Louzada et al., 2011; Reznik et al., 2016; Tikoo et al., 2015). This interest results from the observation that magnetic anomaly lows are ubiquitous phenomena of many impact structures on Earth and Mars (e.g., Acuña et al., 1999; Pilkington & Grieve, 1992). As magnetic susceptibility and remanent magnetization are found well below regional levels in many impacted rocks, extensive alteration is assumed to cause a destruction of magnetic phases. However many studies on impacted rocks since the 1990s have demonstrated that alteration of magnetic minerals must not be the prime reason for magnetic anomaly lows, but the shock itself contribute significantly to the demagnetization mechanism (e.g., Kontny & Grothaus, 2017; Louzada et al., 2011; Reznik et al., 2016).

Magnetite (Fe₃O₄) is an important magnetic mineral in impacted terrestrial rocks (e.g., Gattacceca et al., 2007; Pohl et al., 2010). An earlier study on magnetic and microstructural changes in multidomain magnetite shocked to pressures of 5, 10, 20 and 30 GPa (Reznik et al., 2016, 2017) revealed an overlap of permanent brittle and plastic deformation along with initial amorphization beginning at 20 GPa. These features mainly control the permanent bulk magnetic property changes. However this study also indicated that stress-sensitive features like lattice distortion can be observed near the Verwey transition temperature (T_V). Carporzen and Gilder (2010) observed for decompressed stoichiometric magnetite in the pressure range up to 5 GPa an increase of T_V of 1 K/GPa and postulated a strain memory effect in shocked magnetite. Reznik et al. (2016) suggested that strain memory saturation occurs by 5 GPa because their shocked samples from the pressure range 5 to 30 GPa all show an increase of about 6 K compared to the regular T_V at 120 K. This observation suggests a noticeable stress-sensitivity of T_V in the low shock pressure range.

Annealing is known to considerably reduce internal stress related to dislocations or surficial maghemite formation (γ-Fe₂O₃, the fully oxidized equivalent of magnetite) (e.g., Liu et al., 2008). Therefore the effect of

annealing, either due to the heat produced by the shock itself or by later hydrothermal systems is of high relevance in the understanding of impact-induced magnetic property changes. Potential heat sources for creating an impact-generated hydrothermal system are impact melt rock and impact melt-bearing breccia (suevite), and elevated geothermal gradients in central uplifts (e.g., Osinski et al., 2013; Zürcher & Kring, 2004). Heat treatment of 973–1,073 K of unshocked and shocked iron meteorites produced significantly different microstructures because of collision-induced stresses in the shocked iron meteorites (Jain & Lipschutz, 1968). Such high temperatures are likely produced in regions where shock pressures reached >30 GPa and/or cooling impact melt sheets occur in large impact craters such as e.g., the well-preserved Chicxulub impact structure, Mexico (e.g., Morgan et al., 2016; Ugalde et al., 2005).

The aim of this follow up article to Reznik et al. (2016) is to explore the chemical and magnetic stability of experimentally shocked magnetite after subsequent high-temperature (973 K) treatment above the magnetite Curie temperature (853 K) with special emphasis on the role of stress-induced microstructures. In addition to low- and high-temperature magnetometry and hysteresis properties, particular focus is placed on the identification of the iron oxidation state and its coordination geometry. For this purpose, X-ray powder diffraction (XRD) and high-resolution scanning electron microscopy (HRSEM) was combined with synchrotron-assisted X-ray absorption spectroscopy (XAS).

2. Materials and Methods

Details on the studied material, shock experiments as well as magnetic, X-ray diffraction (XRD) measurements and high-resolution scanning electron microscopy (HRSEM) were recently described by Reznik et al. (2016, 2017). Briefly, a quartz-magnetite banded iron ore (Sydvaranger mine, Norway) containing multidomain magnetite was subjected to shock recovery experiments using an air gun and high-explosives (Langenhorst & Hornemann, 2005). Heating experiments in an argon atmosphere as well as the measurement of the Curie point of magnetite were carried out using a KLY-4S Kappabridge (AGICO) with a heating/cooling rate of about 10 K/min. The effect of heating on the magnetic properties was controlled by measuring the Curie temperature, Verwey transition temperature and saturation isothermal remanent magnetization (SIRM) behavior. SIRM measurements were performed at the Institute for Rock Magnetism (IRM, Minneapolis, USA) using a MPMS 2 SQUID magnetometer and a magnetic field of 2.5 T at 300 K for the sample saturation. Lattice parameter and size of apparent crystallites were analyzed by XRD using a Kristalloflex D500 diffractometer (Siemens).

In contrast to time-consuming high-resolution transmission electron microscopy, HRSEM allows an extraordinary possibility for a rapid and artifact-free access for a spatial identification of morphological and structural changes occurring at the nm-scale (Reznik et al., 2016, 2017). For this purpose, powder of the annealed samples were coated with a 5 nm thick Pt-Pd conductive layer and afterward investigated using a LEO Gemini 1530 SEM microscope coupled with a Thermal Scientific energy-dispersive X-ray analyzer.

The iron oxidation states were studied using a synchrotron-assisted X-ray absorption spectroscopy (XAS) at the SUL-X beamline of the ANKA source (KIT, Karlsruhe, Germany) equipped with a Si (111) crystal pair monochromator. For the K-edge X-ray absorption near edge spectroscopy (XANES) in transmission mode the Fe content was adjusted to an optimal absorption length resulting in an edge jump of between 0.3 and 0.9. For the preparation of pressed pellets about 7 weight percent of cellulose binder was mixed with one weight percent of gently crushed samples. Transmission mode with ionization chambers as detectors was used for acquiring the Fe K-edge XAS spectra. The energy was calibrated at the Fe K-edge lying at 7,112 eV using a 3 μm thick Fe foil mounted between the second and third ionization chamber. Up to three scans have been acquired from two different sample positions while the analyzed sample area was about 100 μm x 100 μm . Prior to the Fe K-edge, the typical scan ranges are from 150 to 50 eV with a 5 eV energy step width and from 50 to 20 eV with a 2 eV step width while in the edge region (between 7,092 and 7,142 eV) the step width has been decreased to 0.3 eV, and above the edge (EXAFS region) a step width of 0.5 eV was selected. Each scan was measured during 1 s, increasing with $k = 0.5$ eV above the edge. The Athena program of the IFFEFIT package (Ravel & Newville, 2005) was used for the pre-edge and post-edge background correction and normalization treatments. The XANES spectra of the studied samples were compared with the reference spectra of magnetite (Fe_3O_4), maghemite ($\gamma\text{-Fe}_2\text{O}_3$) and hematite (Fe_2O_3) obtained with similar parameters taken from the SUL-X reference database as well as with spectra of Fe-bearing minerals/

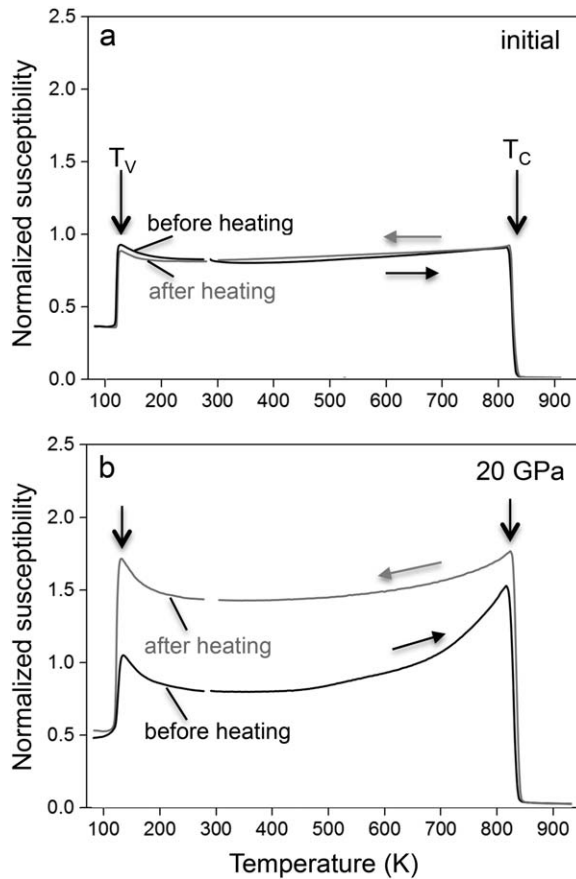


Figure 1. Effect of shock pressure and subsequent heating on Verwey transition (T_V) and Curie point (T_C). (a) Curves of an initial, “0 GPa” sample. Note that the heating (black) and cooling (grey) curves are nearly reversible. (b) Representative irreversible curves for a shocked sample. Curves are normalized to susceptibility values measured at room temperature. “before heating” and “after heating” in the low-temperature curve means measurement before and after heating to 973 K. Vertical arrows indicate amplitude and temperature shifts of peaks at T_V and T_C . (s. also Figure 2 for magnetic transition temperatures of all investigated samples).

seen in the hysteresis parameters and low-temperature SIRM measurements (see Figures 3 and 4; Reznik et al., 2016). However, the HPR calculated from the cooling curve is significantly lower and relatively constant (between 1.21 and 1.24), and does not mirror the progression found in the heating curve. This behavior clearly indicates a modification of magnetic domain state during heating up to 973 K.

We also calculated a Verwey transition peak ratio ($T_V P = k_{max}/k_{10}$, k_{10} is the magnetic susceptibility measured at 10°C/283 K) and found for the initial, multidomain magnetite very similar values before (1.12) and after (1.09) heating (Figure 2d). The shocked samples show significantly higher values (1.31 – 1.36) and relatively constant lower values (1.19–1.22) after heating to 973 K. It is interesting to note that after heating a similar state in all shocked samples seems to be conserved (Figure 2d) mirroring the behavior of the HPR.

These observations indicate that HPR as well as $T_V P$ calculated from k-T curves are suitable parameters to derive changes in the magnetic domain state during heating experiments. The irreversibility of the heating and cooling curves suggests that even if the heating at 973 K was held only for minutes it causes annealing of crystal defects as well as unpinning and increase in volume size of magnetic domains (see next chapters).

3.2. Hysteresis Parameters

Hysteresis parameters measured of shocked magnetite before and after k-T cycling both display hysteresis ratios, which indicate a general pseudo-single domain behavior (Figure 3). But Figure 3 also confirms a

compounds investigated by Wilke et al. (2001), Boubnov et al. (2015), and Bajt et al. (1994). Similarly, as it is described elsewhere (Bajt et al., 1994; Boubnov et al., 2015), the Fe oxidation state and its coordination number were examined by analyzing the centroid position of the Fe-K pre-edge against the Fe^{3+} /total Fe ratio.

3. Results

3.1. Temperature-Dependence of Weak-Field Magnetic Susceptibility

The effect of shock pressure on temperature-dependent magnetic susceptibility (k-T curve) in magnetite is shown in Figure 1. For magnetite shocked between 5 and 30 GPa, we found an irreversible behavior between the heating and cooling curve (representative 20 GPa sample is shown in Figure 1b).

Curie temperatures of all samples determined from the heating curves are at 861 ± 2 K (Figure 2a) indicating that no modification of composition and no oxidation of magnetite occurred. Verwey transition temperatures are 4–6 K higher in the shocked samples than in the initial magnetite (Figure 2b; Reznik et al., 2016). The most obvious features of shocked magnetite compared to the initial magnetite are the development of peaks above the Verwey transition and below the Curie temperature (Figure 1). This feature is in accordance with a transition of multidomain to pseudo-single domain behavior from initial to shocked magnetite, which is already established by hysteresis measurements, FORC distribution diagrams and low-temperature SIRM measurements (Reznik et al., 2016).

Dunlop (2014) has shown that k-T curves of magnetite have the potential to indicate pseudo-single domain behavior and described an “upward progression of peak heights in heating curves” with decreasing grain size. In his study, this behavior was mirrored in the cooling curve. Comparing the Hopkinson peak ratio ($HPR = k_{max}/k_{40}$, k_{40} is the magnetic susceptibility measured at 40°C/313 K) of initial and shocked magnetite from our k-T curves (Figure 2c) we observe a clear increase from 1.12 in the initial sample up to 1.9 in the 20 GPa shocked sample in agreement with magnetic grain size reduction

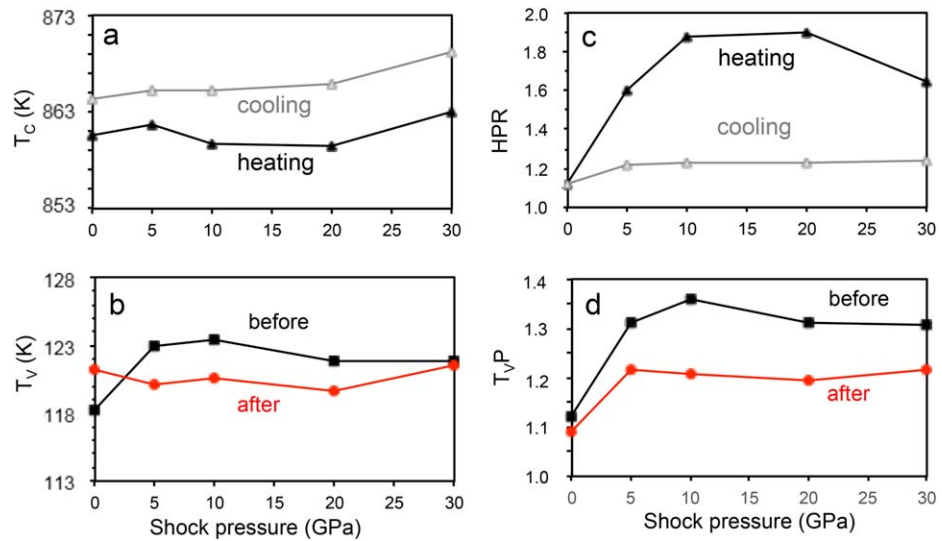


Figure 2. Effect of shock pressure and subsequent heating on characteristic magnetic transitions. (a) Curie temperature (T_c) and (b) Verwey transition temperature (T_v) determined from the first derivative of temperature-dependent magnetic susceptibility curves (see Figure 1). In (a) black triangles are from heating and open grey triangles from cooling curves. In (b) black squares denote sample pieces measured before and red circles those samples after temperature cycling. (c) Hopkinson peak ratio (HPR) from heating (black triangle) and cooling (open grey triangle) curve. (d) Verwey transition peak ratio (T_vP) before and after temperature cycling. See text for details.

change in magnetic domain size toward a more multidomain magnetic behavior, especially for the heated 10 and 20 GPa sample. This observation clearly indicates a change in magnetic domain size during the heating experiments, which is most likely associated with the annealing of lattice defects. It is interesting to note that the saturation magnetization (M_s) of three of the four shocked samples increase after the heating experiment (see Table 1) after they significantly decreased due to the shock experiments (Reznik et al., 2016). This observation would be in line with a recovery of magnetite from an amorphous to a crystalline state or even a nucleation of new magnetite grains. Patches of amorphous-like magnetite are documented in the shocked magnetite by transmission electron microscopy (Reznik et al., 2016).

3.3. Low-Temperature SIRM

Figure 4 presents cooling and warming cycles of low-temperature SIRM acquired in a strong external magnetic field at room temperature (RT). The initial sample (Figure 4a) exhibits a sharp Verwey transition around 120 K, which is typical for magnetite. Compared to the initial sample, the Verwey transition loses its sharpness in the shocked and subsequent heated samples (Figures 4b–4e). However the shape of all RTSIRM curves is typical for magnetite and no noticeable traces of maghemite are recognized, which would produce hump-shaped peaks around 200 K (Özdemir & Dunlop, 2010). All samples show a loss in remanence through T_v on cooling. Below T_v some of the shocked samples (5 and 10 GPa) show a faint second T_v around 100 K, which vanishes in the warming curve.

The amount of recovered magnetic memory acquired after a cooling-warming cycle can be determined using the ratio of SIRM at 300 K before and after the measurement (for definition of magnetic memory ratio; see e.g., Bowles et al., 2012 and Reznik et al., 2016). Figures 4a and 4f show that the magnetic memory ratio of initial magnetite is about 20%, typical for multidomain magnetite. Especially above 10 GPa the magnetic memory ratio considerably improved to values up to 53%, indicating an increasing ability of shocked magnetite to

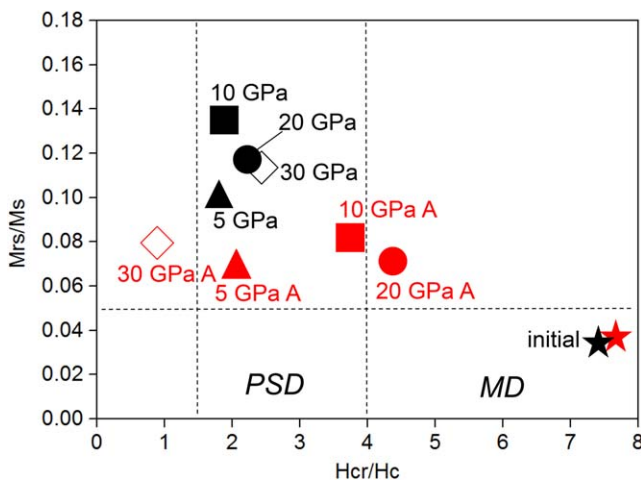


Figure 3. Effect of shock pressure and subsequent 973 K heating on M_{rs}/M_s and H_{cr}/H_c ratios (after Day et al., 1977). Note that heating partially erases the shock-induced domain refinement (data for shocked magnetite are from Reznik et al., 2016).

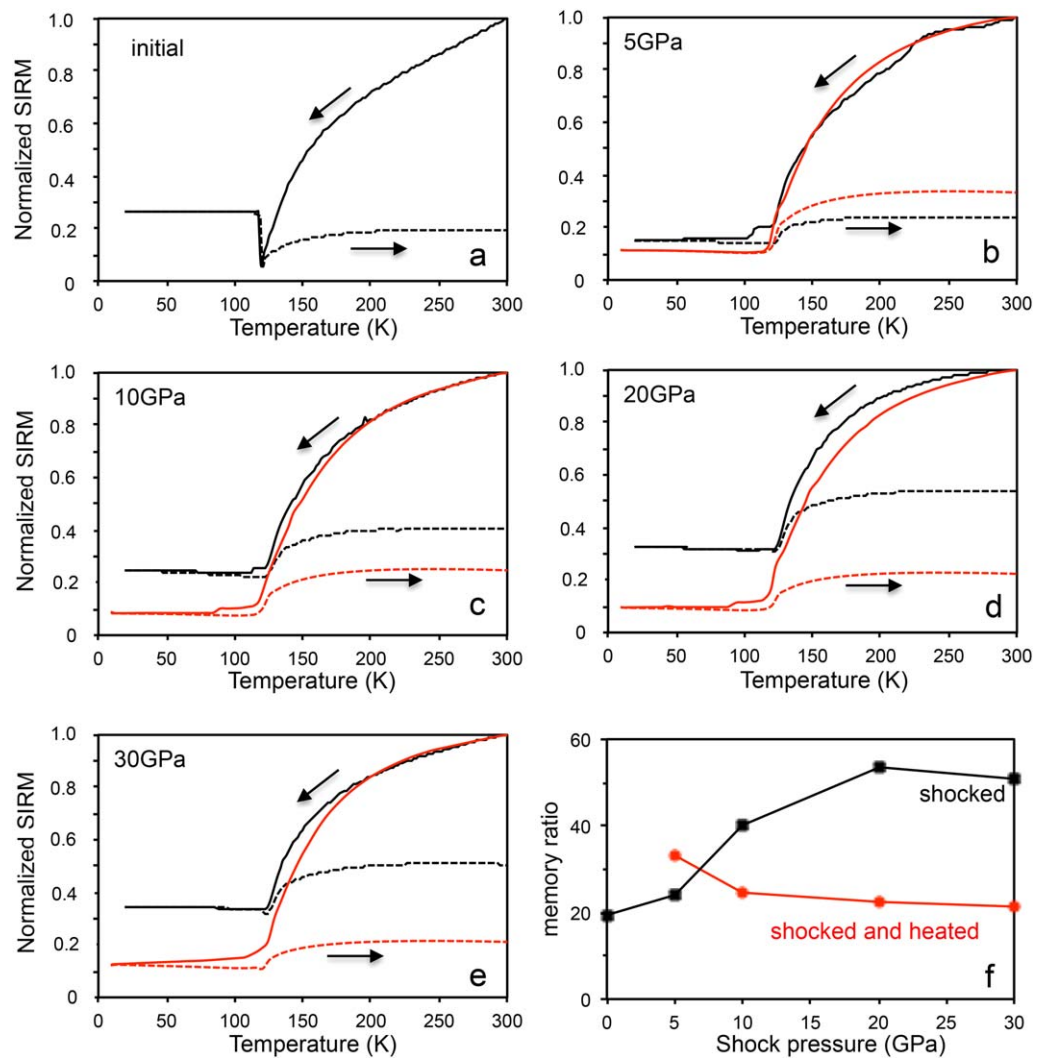


Figure 4. Low-temperature cooling-warming cycling of SIRM (normalized to 300 K) versus temperature for cooling and warming cycle. (a) Initial multidomain magnetite, (b-e) shocked (black) and afterward heated at 973 K (red). Solid line: cooling curve, dotted line: warming curve. Data shown in black in a-e are from Reznik et al. (2016). (f) Memory ratio calculated from SIRM acquired after a cooling-warming cycle for initial, shocked and shocked magnetite after k-T measurement (shocked and heated).

Table 1

Hysteresis Parameter of Initial, Shocked, and Afterward Annealed (A) Magnetite Ore (Data for Shocked Magnetite are From Reznik et al., 2016)

Specimen	M_s (Am^2/kg)	M_{rs} (Am^2/kg)	H_c (mT)	H_{cr} (mT)	M_{rs}/M_s	H_{cr}/H_c
Initial	58.61	1.99	1.52	11.82	0.034	7.776
Initial A	56.85	2.13	1.50	11.80	0.037	7.867
5 GPa	34.52	3.54	8.14	15.00	0.103	1.843
10 GPa	44.21	5.83	16.03	31.60	0.132	1.971
20 GPa	42.35	5.12	17.28	36.83	0.121	2.131
30 GPa	12.76	1.53	18.04	39.30	0.120	2.178
5 GPa A	43.24	2.92	4.52	9.84	0.068	2.178
10 GPa A	39.35	3.18	3.42	13.24	0.081	3.872
20 GPa A	76.83	5.22	2.79	12.33	0.068	4.417
30 GPa A	28.59	2.29	5.29	6.05*	0.080	0.950

acquire a laboratory magnetic remanence. Figure 4 also shows that the magnetic memory ratio of shocked magnetite after heating reaches values comparable to those of the initial magnetite in line with a magnetic domain size recovery. The only exception is seen in the 5 GPa sample (Figure 4b), which shows a 10% higher magnetic memory after heating than the shocked one.

3.4. XRD Data

The X-ray diffractograms of the shocked and afterward heated magnetite (Figures 5a and 5b) contain characteristic Fe_3O_4 peaks with no measurable contributions from maghemite or hematite in agreement with the magnetic measurements. The unit cell volume for the initial magnetite (590.0 Å) is very close to the published value 589.1 Å for synthetic magnetite (Strunz, 1982) while it is lower compared to values (592.25 and 591.35 Å) reported for natural magnetite (Henderson et al., 2007). Therefore the natural magnetite from a high-grade metamorphic iron ore used for this study is rather pure and stoichiometric (description of starting material and shocked magnetite is given in Reznik et al., 2016).

After heating, both, quartz and magnetite peaks become sharper compared to the shocked ones. While the shock provokes a decrease in the unit cell volume, heating to 973 K of the shocked magnetite brings the unit cell volume back to its previous values (Figure 5c) and causes a recovery. These changes in the lattice parameter appear to be reversible and independent from the applied shock pressure.

In contrast, the apparent crystallite size values exhibit a higher sensitivity to the variations in both, shock pressure and heating (Figure 5d). While the apparent crystallite size of shocked magnetite is strongly reduced due to grain fragmentation and crystal defects (Reznik et al., 2016), the heated and shocked magnetite shows a less strong pronounced decrease of the apparent crystallite size compared to the initial magnetite. However, the original apparent crystallite size values are not reached any more suggesting the presence of irreversible shock-induced transformations (fragmentation and other microstructures). The apparent size of the coherent crystallites increased in comparison to the shocked magnetite and depends on the pretreatment shock pressure. This behavior is in agreement with a recovery of lattice defects.

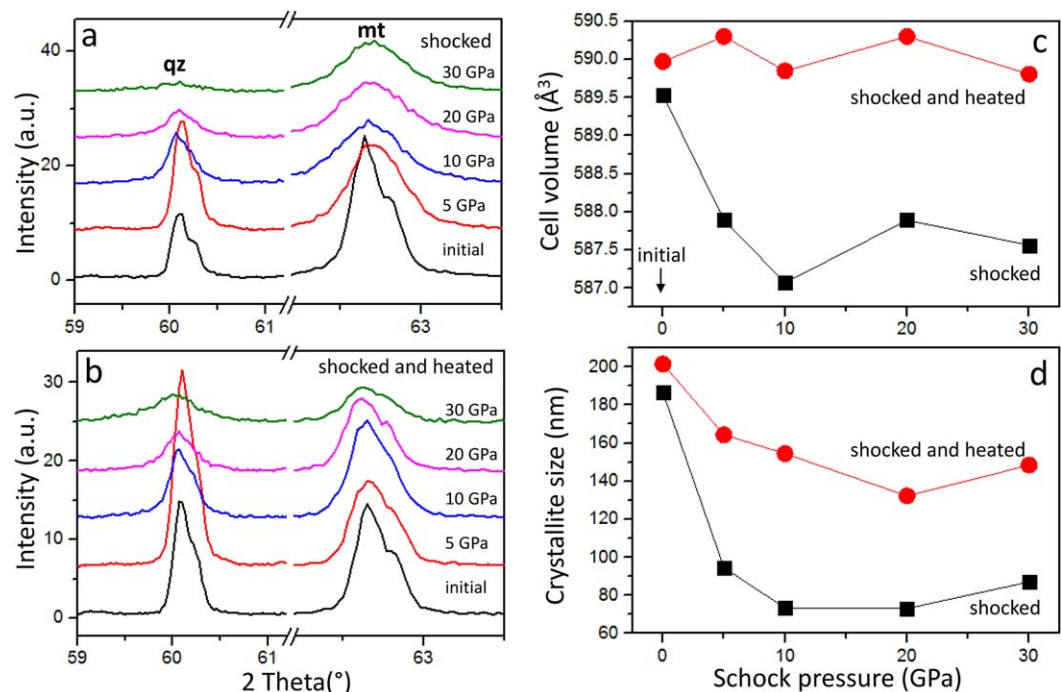


Figure 5. Effect of shock pressure and subsequent 973 K heating on the evolution of the diffraction pattern in magnetite. High-angle diffraction area (a) from shocked and (b) from shocked and subsequent heated samples containing (21-1) quartz (qz) and (440) magnetite (mt) peaks. Variation of (c) cell volume and (d) apparent crystallite size. Data for shocked samples are from Reznik et al. (2016).

3.5. High-Resolution Scanning Electron Microscopy

The fracture plane morphology of the heated initial and shocked magnetite from representative HRSEM observations is shown in Figure 6. Nano-sized pores containing Fe-Mg-Al-silicate residues at the pore rims were identified in all heated samples (Figures 6a and 6b). All annealed samples are also characterized by the presence of smoothed plane edges and fracture terraces while tiny shear bands still occur in the shocked samples (Figures 6c and 6d). In the 20 and 30 GPa sample new formation of nano-sized grains along microfractures and high-angle grain boundaries on crystal planes of the former shocked magnetite were observed (Figures 6e and 6f). The latter clearly indicates recrystallization of the shocked magnetite during the short heating duration. The mosaic grains are about 100 nm in size. It is interesting to note that the recrystallization is only observed in the higher shocked sample and not in the initial or low shock magnetite.

3.6. K-Edge XANES Data

Figure 7 presents the results of XANES investigations of iron oxidation state and its local atomic coordination. The XANES spectra exhibit two prominent peaks in the absorption edge region. The main peak at around 7,130 eV (Figure 7a) is related to the absorption edge where tetrahedral and octahedral coordinated Fe atoms contribute together. Because twice as much octahedral compared to tetrahedral sites occur, this peak is mainly controlled by octahedral site occupation with an equal amount of Fe²⁺ and Fe³⁺. The pre-edge feature at about 7,113 eV is dominated by tetrahedrally coordinated Fe³⁺ although all three oxidation states and coordination numbers (VI Fe²⁺, IV Fe³⁺, VI Fe³⁺) can contribute (e.g., Wilke et al., 2001).

The shape of the XANES peaks and their energetic positions (Figure 7a) indicate that all studied samples correspond to a relatively well-crystallized magnetite and do not show any significant structural or electronic changes (e.g., Baudalet et al., 2010; Wilke et al., 2001). Compared to the shocked samples (black

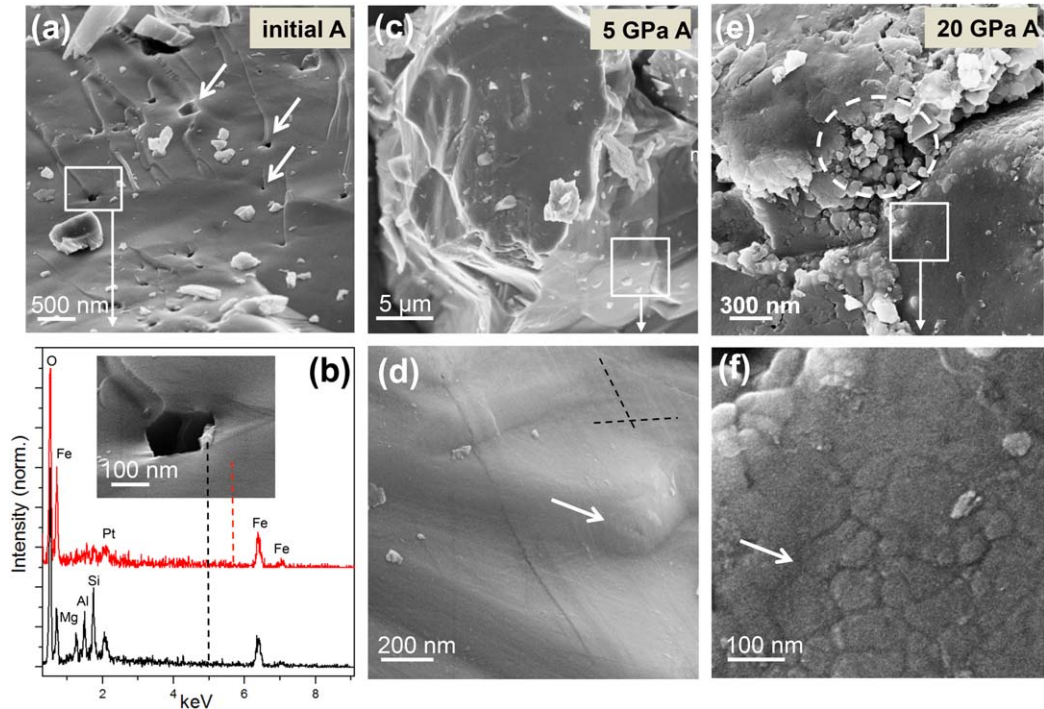


Figure 6. HRSEM observations of initial and shocked magnetite grains after heating. (a) A net of nano-sized pores is shown in the initial sample. (b) The magnified area from (a) and the EDX analysis show the dissolution/degassing of a Fe-Mg-Al-bearing silicate like e.g., chlorite in magnetite. Pt peak is from coating the sample with a 5 nm thick Pt-Pd conductive layer. (c, d) Shear bands are still observable in the 5 GPa sample (dashed lines) but edges are smoothed (arrow in Figure 6d). (e) Nucleation of nano-sized magnetite grains along microfractures (dashed circle). (f) Magnification from Figure 6e shows high-angle grain boundaries (around 120°) in the 20 GPa sample. Compare with initial and shocked microstructures given in Reznik et al. (2016, 2017).

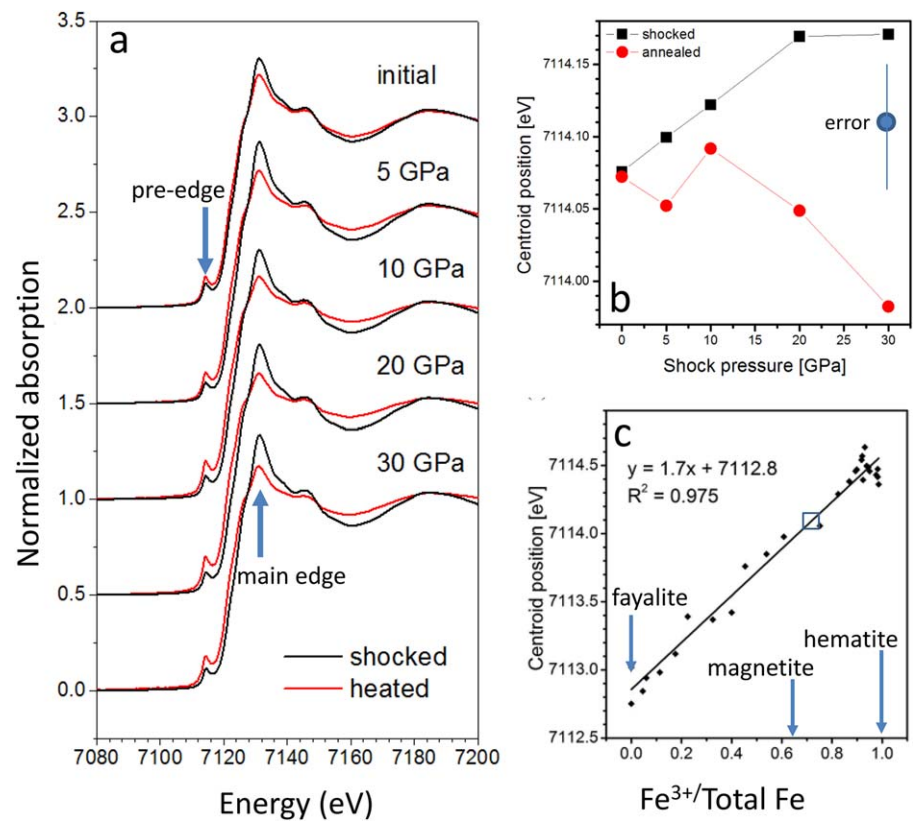


Figure 7. XANES analysis of oxidation states. (a) Fe K-edge XANES spectra for initial, shocked (black curves) and subsequently heated samples (red curves). (b) Centroid position of the pre-edge peak as a function of the shock pressure (black symbols) and the subsequent heating (red symbols). (c) Calibration curve (from Boubnov et al., 2015) shows a linear relationship between the centroid position of the preedge peak for hematite ($\text{Fe}^{3+}/\text{Total Fe} = 1$), magnetite ($\text{Fe}^{3+}/\text{Total Fe} = 0.67$) and synthetic fayalite, Fe_2SiO_4 ($\text{Fe}^{3+}/\text{Total Fe} = 0$). Blue arrows indicate position of reference oxides according to Bajt et al. (1994) while the blue frame shows data of this study shown in Figure 7b.

curves), small changes in intensities of absorption peaks occur in the annealed samples (red curves) which might be artifacts and do not indicate any chemical changes.

The centroid position of the preedge peak is very sensitive to changes in oxidation state, in particular to the variation of the $\text{Fe}^{3+}/\text{Total Fe}$ ratio (see e.g., Bajt et al., 1994; Boubnov et al., 2015). By taking into account the value of the experimental energetic error (~ 0.1 eV in Figure 7b) it can be concluded that after heating the centroid position is nearly the same for the initial samples and also for the 5 and 10 GPa samples (before and after heating). However, the heated samples, which were previously shocked at 20 and 30 GPa show a slight drop of the centroid position. Nevertheless this change is very small and comparing our data ($\text{Fe}^{3+}/\text{Total Fe}$ ratio is between about 0.70 and 0.75) with the calibration curve for the $\text{Fe}^{3+}/\text{Total Fe}$ ratio of Boubnov et al. (2015) (Figure 7c), initial, shocked and subsequently heated samples are all located close to the magnetite position ($\text{Fe}^{3+}/\text{Total Fe}$ ratio = 0.67; see Bajt et al., 1994) albeit little alteration of magnetite is indicated for all samples independent of treatment.

4. Discussion and Conclusions

We investigated in this study the effect of heating of previously shocked magnetite from a metamorphic magnetite-quartz banded iron ore on magnetic and mineralogical properties in order to better understand impact-induced magnetic features. Compared to the initial magnetite, the shocked magnetite for our heating experiments show a significant decrease in magnetic susceptibility, an increase in saturation isothermal remanent magnetization and in the magnetic memory in agreement with a multidomain to pseudo-single magnetic domain transition. In addition a decrease in the apparent crystallite size was observed (Reznik

et al., 2016). The magnetic domain size reduction was shown to be either the effect of grain fragmentation or pinning of domain walls at crystal defects and dislocations. Changes of lattice parameters along with an increase in width and temperature of the Verwey transition suggests also a distortion of the tetrahedral and octahedral crystal sites and internal stresses (Reznik et al., 2016).

Heating of the shocked magnetite modifies the intrinsic magnetic properties and suggests a significant ability for magnetic changes in impacted rocks even after a short heat treatment of only a few minutes. The most obvious change is an increase in the volume size of magnetic domains, which is documented by hysteresis properties (Figure 3), SIRM magnetic memory (Figure 4f) and temperature-dependent magnetic susceptibility (Figures 1b and 2c). These observations agree well with the growth of the apparent crystallite size in the shocked and heated magnetite suggesting a recovery of lattice defects (Figure 5d). The recovery process is documented in our study by recrystallization of magnetite producing a mosaic texture of about 100 nm in size, and nucleation of new magnetite nano-grains along microfractures during heating (Figures 6e and 6f). These microstructures are in accordance with a diffusion creep mechanism in magnetite (e.g., Till & Moskowitz, 2013) during the short heating time of our experiments. Recovery of lattice defects seems to be accompanied by a relaxation of a slightly distorted lattice of the shocked magnetite, which is constrained by the change in the unit cell volume (Figure 5c). This observation agrees with earlier studies of Jain and Lipschutz (1968) on heating experiments of unshocked and shocked iron meteorites. Similar mosaic textures to those shown in Figure 6f were only observed in previously shocked samples. Indeed they also noted differences in textures depending on the shock-loading history and interpreted these differences to be a function of the degree of disordering in the higher shocked samples. Jain and Lipschutz (1968) suggested that the thermal release of stresses is the driving force for the different textures.

Reznik et al. (2016) already described the exceptional decrease in M_s in the shocked compared to the initial magnetite. They speculated that the main reasons for this decrease were internal stress, amorphization and a high concentration of surface defects along shear bands and twin boundaries. The partial recovery of M_s after heating in our follow up study actually confirm this hypothesis and it looks like that a recovery of the lattice is indeed able to make a significant effect on M_s .

Temperature-dependent magnetic susceptibility measurements above the Curie temperature of shocked magnetite indicate that this method is a powerful tool to identify intrinsic features that can be reversed by heating such as mechanical stress and lattice defects. These features are, in turn, responsible for the increase of coercivity of shocked ferrimagnetic minerals (e.g., Mang et al., 2013; Reznik et al., 2016). Liu et al. (2008) reported that annealing of multidomain magnetite "can significantly reduce internal stress caused by dislocations or surficial maghemite rims," and the latter effect is especially effective if grains are small due to their volume percentage. In Reznik et al. (2016) we already suspected that the faint second T_V at around 100 K (Figure 4) might be related to some degree of distortion in the magnetite lattice. T_{VS} around 100 K has also been observed in shocked magnetite from impacted rocks (e.g., Kontny & Grothaus, 2017; Mang & Kontny, 2013) and are suggested to indicate a small amount of vacancies and increased Fe^{3+} concentration in surface layers of magnetite grains. The heated shocked 10, 20 and 30 GPa samples show an even stronger irreversibility below T_V .

To even better understand the internal stress mechanism and possible chemical changes (e.g., maghemitization) we also investigated the Fe oxidation state ($Fe^{3+}/Total\ Fe$ ratio) and its coordination geometry by synchrotron-assisted X-ray absorption spectroscopy. The XANES data unambiguously demonstrate that all studied samples correspond to magnetite and no traces of maghemite or hematite were detected albeit surface oxidation would not be seen as XANES probe the bulk and the normalized spectrum is an average state of all probed iron atoms. However the $Fe^{3+}/Total\ Fe$ ratio of between 0.70 and 0.75 indeed indicates a very small alteration already of the initial magnetite (compared to 0.67 for pure magnetite; Bajt et al., 1994), which also explains the slightly lower unit cell volume of our initial magnetite (590.0 Å; published data for natural magnetite: 592.25 Å, 591.35 Å in Henderson et al., 2007). Therefore all applied magnetic and mineralogical methods indicate that magnetite is the only relevant magnetic iron oxide in our samples. The fact that the centroid position in the annealed samples, which were previously shocked at 20 and 30 GPa, seems to approach the position of pure magnetite (Figure 7b) suggests that higher shock pressures are accompanied by higher internal stresses. These higher internal stresses are suggested to be the driving force for the observed recrystallization during heating (Figure 6f).

More studies however are needed to investigate the relationship between the peak shock pressure and the annealing parameters such as maximum temperature, heating duration and annealing atmosphere.

In summary, heating of the shocked magnetite ore to 973 K in an argon atmosphere is characterized by a number of irreversible features including

1. significantly higher magnetic susceptibility,
2. Hopkinson peak ratio, which is significantly higher in the heating than in the cooling curve,
3. Verwey transition peak ratio, which is higher in shocked samples compared to shocked and afterward heated samples,
4. Verwey transition temperature, which is slightly reduced in shocked and afterward heated samples,
5. lower coercivity in heated magnetite compared to those, which were only shocked,
6. not fully recovery of apparent crystallite sizes (XRD) agrees with the observation that shock-induced microstructures still occur,
7. recrystallization only occurs in the higher shocked (20 and 30 GPa) and not in the initial or low shocked (5 GPa) magnetite.

The observed annealing effects from this study might have severe consequences on magnetic properties of impacted material and related magnetic anomalies of large impact craters on Earth and across the solar system if at the time of the impact event a magnetic field was active. The Chicxulub impact structure (diameter ca. 200 km, Mexico), for instance is characterized by a pronounced gravity and magnetic anomaly, which is interpreted in terms of a multi-ring structure. It was suggested that the magnetic highs either consist of basement material brought up in the central uplift/peak ring, or of impact melt (Pilkington & Hildebrand, 2000). A joint drilling expedition by IODP and ICDP (expedition 364) sampled the peak ring of the Chicxulub impact structure and found that the peak ring is formed by uplifted fractured and shocked felsic basement rocks overlain by impact melt rock and impact breccia (Morgan et al., 2016). A thermal model of the post-impact hydrothermal system of the Chicxulub impact structure suggests a possible activity of 1.5 to 2.3 Myr (Abramov & Kring, 2007) with excess temperatures of 623 K in a first metasomatic stage (Zürcher & Kring, 2004). Primary ilmenite-magnetite-pairs from impact melt fragments of the ICDP Yaxcopoil-1 drill core were used to constrain the impact melt emplacement temperature ($1,033 \pm 40$ K) (Zürcher & Kring, 2004). Therefore 973 K heating temperatures used in our study is likely placed at the high temperature end member of impact generated heat systems. Filling the temperature space between these two estimates will help to constrain the effect of annealing on rock magnetic property changes and may help to explain magnetic anomaly highs in large impact craters on Earth.

Acknowledgments

This work was funded by the SPP "Planetary Magnetism" of the DFG (KO1514/8-1). We thank the IRM Minneapolis for a research fellowship to BR and especially Mike Jackson for his kind support. Many thanks to Stuart Gilder who provided some missing hysteresis data. Beate Ötzel is thanked for XRD measurements. We acknowledge the constructive and very helpful reviews of Bruce Moskowitz and an anonymous reviewer. Magnetic, XRD and XANES data for the production of figures in this article are given in a supporting information.

References

- Abramov, O., & Kring, D. A. (2007). Numerical modeling of impact-induced hydrothermal activity at the Chicxulub crater. *Meteoritics & Planetary Science*, 42(1), 93–112.
- Acuña, M. H., Connerney, J. E. P., Ness, N. F., Lin, R. P., Mitchell, D., Carlson, C. W., et al. (1999). Global distribution of crustal magnetization discovered by the Mars Global Surveyor MAG/ER experiment. *Science*, 284, 5415–5427.
- Bajt, S., Sutton, S. R., & Delaney, J. S. (1994). X-ray microprobe analysis of iron oxidation states in silicates and oxides using X-ray absorption near edge structure (XANES). *Geochimica et Cosmochimica Acta*, 58(23), 5209–5214.
- Baudelet, F., Pascarelli, S., Mathon, O., Itié, J. P., Polian, A., & Chervin, J. C. (2010). Absence of abrupt pressure-induced magnetic transitions in magnetite. *Physics Review B: Condensed Matter and Materials Physics*, 82(14), 140412-1–140412-4.
- Bezaeva, N. S., Swanson-Hysell, N. L., Tikoo, S. M., Badyukov, D. D., Kars, M., Egli, R., et al. (2016). The effects of 10 to >160 GPa shock on the magnetic properties of basalt and diabase. *Geochemistry, Geophysics, Geosystems*, 17, 4753–4771. <https://doi.org/10.1002/2016GC006583>
- Boubnov, A., Lichtenberg, H., Mangold, S., & Grunwaldt, J. D. (2015). Identification of the iron oxidation state and coordination geometry in iron oxide- and zeolite-based catalysts using pre-edge XAS analysis. *Journal of Synchrotron Radiation*, 22(2), 410–426. <https://doi.org/10.1107/S1600577514025880>
- Bowles, J., Jackson, M., & Brown, L. (2012). The magnetite Verwey transition. *irm Q*, 22(2), 1–12.
- Carporzen, L., & Gilder, S. A. (2010). Strain memory of the Verwey transition. *Journal of Geophysical Research*, 115, B05103. <https://doi.org/10.1029/2009JB006813>
- Day, R., Fuller, M., & Schmidt, V. A. (1977). Hysteresis properties of titanomagnetites: Grain-size and compositional dependence. *Physics of Earth and Planetary Interiors*, 13(4), 260–267.
- Dunlop, D. J. (2014). High-temperature susceptibility of magnetite: A new pseudo-single-domain effect. *Geophysical Journal International*, 199(2), 707–716. <https://doi.org/10.1093/gji/ggu247>
- Gattacceca, J., Lamali, A., Rochette, P., Boustie, M., & Berthe, L. (2007). The effects of explosive-driven shocks on the natural remanent magnetization and the magnetic properties of rocks. *Physics of Earth and Planetary Interiors*, 162(1–2), 85–98. <https://doi.org/10.1016/j.pepi.2007.03.006>
- Henderson, C. M. B., Charnock, J. M., & Plant, D. A. (2007). Cation occupancies in Mg, Co, Ni, Zn, Al ferrite spinels: A multi-element EXAFS study. *Journal of Physics: Condensed Matter*, 19(7), 076214. <https://doi.org/10.1088/0953-8984/19/7/076214>

- Jain, A. V., & Lipschutz, M. E. (1968). Implications of shock effects in iron meteorites. *Nature*, 220(5163), 139–143.
- Kontny, A., & Grothaus, L. (2017). Effect of shock pressure and temperature on titanomagnetite from ICDP cores and target rocks of the El'gygytgyn impact structure, Russia. *Studia Geophysica et Geodaetica*, 61(1), 162–183. <https://doi.org/10.1007/s11200-016-0819-3>
- Langenhorst, F., & Hornemann, U. (2005). Shock experiments on minerals: Basic physics and techniques. *EMU Notes in Mineralogy*, 7(15), 357–387.
- Liu, Q., Yu, Y., Muxworthy, A. R., & Roberts, A. P. (2008). Effects of internal stress on remanence intensity jumps across the Verwey transition for multi-domain magnetite. *Physics of the Earth and Planetary Interiors*, 169(1–4), 100–107. <https://doi.org/10.1016/j.pepi.2008.07.008>
- Louzada, K. L., Stewart, S. T., Weiss, B. P., Gattacceca, J., Lillis, R. J., & Halekas, J. S. (2011). Impact demagnetization of the Martian crust: Current knowledge and future directions. *Earth and Planetary Science Letters*, 305(3–4), 257–269.
- Mang, C., & Kontny, A. (2013). Origin of two Verwey transitions in different generations of magnetite from the Chesapeake Bay impact structure, USA. *Journal of Geophysical Research: Solid Earth*, 118, 5195–5113. <https://doi.org/10.1002/jgrb.50291>
- Mang, C., Kontny, A., Fritz, J., & Schneider, R. (2013). Shock experiments up to 30 GPa and their consequences on microstructures and magnetic properties in pyrrhotite. *Geochemistry, Geophysics, Geosystems*, 14, 64–85. <https://doi.org/10.1029/2012GC004242>
- Morgan, J. V., Gulick, S. P. S., Bralower, T., Chenot, E., Christeson, G., Claeys, P., et al. (2016). The formation of peak rings in large impact craters. *Science*, 354(6314), 878–882. <https://doi.org/10.1126/science.aah6561>
- Osinski, G. R., Tornabene, L. L., Banerjee, N. R., Cockell, C. S., Flemming, R., Izawa, M. R. M., et al. (2013). Impact-generated hydrothermal systems on Earth and Mars. *Icarus*, 224(2), 347–363. <https://doi.org/10.1016/j.icarus.2012.08.030>
- Özdemir, Ö., & Dunlop, D. J. (2010). Hallmarks of maghemitization in low-temperature remanence cycling of partially oxidized magnetite nanoparticles. *Journal of Geophysical Research*, 115, B02101. <https://doi.org/10.1029/2009JB006756>
- Pilkington, M., & Grieve, R. A. F. (1992). The geophysical signature of terrestrial impact craters. *Reviews of Geophysics*, 30(2), 161–181.
- Pilkington, M., & Hildebrand, A. R. (2000). Three-dimensional magnetic imaging of the Chicxulub crater. *Journal of Geophysical Research*, 105(B10), 23479–23491.
- Pohl, J., Poschlod, K., Reimold, W. U., Meyer, C., & Jacob, J. (2010). Ries crater, Germany: The Enkingen magnetic anomaly and associated drill core SUBO 18. *Geological Society of America Special Papers*, 465, 141–163.
- Ravel, B., & Newville, M. (2005). ATHENA, ARTEMIS, HEPHAESTUS: Data analysis for X-ray absorption spectroscopy using IFEFFIT. *Journal of Synchrotron Radiation*, 12(4), 537–541. <https://doi.org/10.1107/S0909049505012719>
- Reznik, B., Kontny, A., & Fritz, J. (2017). Effect of shock waves on magnetic susceptibility and microstructure of a magnetite-bearing ore. *Meteoritics & Planetary Sciences*, 52(7), 1495–1504. <https://doi.org/10.1111/maps.12787>
- Reznik, B., Kontny, A., Fritz, J., & Gerhards, U. (2016). Shock-induced deformation phenomena in magnetite and their consequences on magnetic properties. *Geochemistry, Geophysics, Geosystems*, 17, 2374–2320. <https://doi.org/10.1002/2016GC006338>
- Strunz, H. (1982). *Mineralogische tabellen* (621 pp.). Leipzig, Germany: Akademische Verlagsgesellschaft.
- Tikoo, S. M., Gattacceca, J., Swanson-Hysell, N. L., Weiss, B. P., Suavet, C., & Cournède, C. (2015). Preservation and detectability of shock-induced magnetization. *Journal of Geophysical Research: Planets*, 120, 1461–1475. <https://doi.org/10.1002/2015JE004840>
- Till, J. L., & Moskowitz, B. (2013). Magnetite deformation mechanism maps for better prediction of strain partitioning. *Geophysical Research Letters*, 40, 697–702. <https://doi.org/10.1002/GRL.50170>
- Ugalde, H. A., Artemieva, N., & Milkereit, B. (2005). Magnetization on impact structures - constraints from numerical modeling and petrophysics. In T. Kenkmann, F. Hörz, & A. Deutsch (Eds.), *Large meteorite impacts III* (Geol. Soc. Am. Soc. Paper, 384, pp. 25–42). Boulder, CO: GSA.
- Wilke, M., Farges, F., Petit, P. E., Brown, G. E., Jr., & Martin, F. (2001). Oxidation state and coordination of Fe in minerals: A Fe K-XANES spectroscopic study. *American Mineralogist*, 86(5–6), 714–730.
- Zürcher, L., & Kring, D. A. (2004). Hydrothermal alteration in the core of the Yaxcopoil-1 borehole, Chicxulub impact structure, Mexico. *Meteoritics & Planetary Science*, 39(7), 1199–1221.